A polymer-physics view of peripheral chromatin: de Gennes' self-similar carpet model

Ozan S. Sarıyer
Pîrî Reis University, School of Arts and Sciences, Tuzla 34940, Istanbul, Turkey[*]

Aykut Erbaş
UNAM National Nanotechnology Research Center and
Institute of Materials Science & Nanotechnology, Bilkent University, Ankara 06800, Turkey
University of Silesia, Institute of Physics, Katowice, Poland[†]

(Dated: January 15, 2024)

Using scaling arguments to model peripheral chromatin localized near the inner surface of the nuclear envelope (NE) as a flexible polymer chain, we discuss the structural properties of the peripheral chromatin composed of alternating lamin-associated domains (LADs) and inter-LADs. Modeling the attraction of LADs to NE by de Gennes' self-similar carpet, which treats the chromatin layer as a polymer fractal, explains two major experimental observations: (*i*) The high density of chromatin close to the nuclear periphery decays to a constant density as the distance to the periphery increases. (*ii*) Due to the decreasing mesh size towards the nuclear periphery, the chromatin carpet inside NE excludes molecules (via non-specific interactions) above a threshold size that depends on the distance from the nuclear periphery.

I. INTRODUCTION

Inside the highly crowded volume of the eukaryotic cell nucleus, chromatin is not randomly distributed [1–7]. While euchromatin, which allows access to lineage-specific genes, is often observed away from the nuclear surfaces, heterochromatin, which is commonly associated with gene silencing, is localized near the nuclear surfaces [4–10]. This 3d organization scheme is also one of the epigenetic factors regulating the biological characteristics and health of a cell [11, 12]. Consistently, many genetic disorders with a terminal nature, such as various types of laminopathies [13–18] and in some cancers [19, 20], manifest themselves as alterations in peripheral chromatin distribution. Understanding the origins of such distorted distribution patterns requires characterizing the structural and conformational properties of peripheral chromatin localized near the inner surface of the nuclear envelope (NE).

Recent progress in sequence-based chromatin conformation capture technologies (e.g., Hi-C [21], ChIP [22], and DamID [23]) in addition to developments in high-resolution-microscopy (e.g., FISH [24]), have provided the most detailed structural properties of peripheral chromatin so far [7, 25]. These experiments report that peripheral chromatin, also referred to as lamina-associated domains (LADs), interact with nuclear boundary components and have the characteristics of gene-inactive heterochromatin. These domains have sharply defined boundaries, and their lengths range between 0.1 Mb (mega-basepairs) to 10 Mb with a median length of about $\sim$ 0.5 Mb [7, 26–31]. LADs are connected by relatively longer strands of inter-LADs, which form chromatin loops protruding towards the nuclear interior (Fig. 1). Interestingly, unlike LADs, inter-LADs exhibit the characteristics of gene-active euchromatin [31–34]. Consistently, experiments reported that large multiprotein complexes maintaining gene transcription (*e.g.*, RNA polymerase II) and enzymes involved in DNA repair machinery (*e.g.*, DNA glycosylase) interact less with LADs than with inter-LADs [7, 9, 26]. Relatedly, experiments probing chromosome structures with nanometer-sized dextran particles showed that large probe particles could not penetrate near the nuclear boundary [35], which suggests a denser (chromatin) environment with smaller mesh sizes at the nuclear periphery, in comparison to central nuclear space.

LADs are anchored to the inner surface of NE (see Fig. 1) via molecular interactions provided by a zoo of lamina-associated proteins such as LBR, LAP1, LAP2β, LEMD2, MAN1, PRR14, *etc.* (see, *e.g.*, Refs. [7, 17, 30] and references therein). As such, given the length of LADs, it is intuitive to think that long strands of LADs bind to the inner-nuclear surface via multivalent molecular contacts, which can provide cumulative interaction energies on the order of $\sim 10\ k_{\rm B}T$ [36, 37] easily, where $k_{\rm B}$ is the Boltzmann constants and T is the absolute temperature. This cumulative attraction strength can stabilize LADs strongly enough that the average distribution of peripheral chromatin may not change drastically during the lifetime of a healthy cell. Notably, a kinetic turnover between surface-attached and non-attached LAD segments can occur. This molecular picture can allow peripheral chromatin to be considered as an adsorbed polymer layer, which can reveal the functional role of peripheral chromatin structures.

In this study, we consider peripheral chromatin as a flexible polymer chain adsorbed onto the NE surface by employing de Gennes' self-similar carpet model. Using

[*] ossariyer@pirireis.edu.tr
[†] aykut.erbas@unam.bilkent.edu.tr

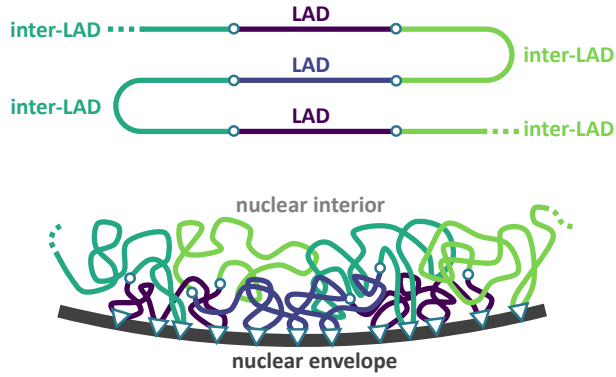

FIG. 1. Authors' view of peripheral chromatin. A polymer train of alternating LADs (purple and blue) and inter-LADs (light and dark green) along a peripheral chromosome. Open circles indicate the sharp LAD/inter-LAD borders. Various proteins anchoring LADs to the nuclear boundary are represented with triangles. The real biological environment at the eukaryotic nuclear periphery may have a higher chromatin density than shown here.

scaling arguments, we estimate the thickness of the LAD layer and relate the polymer nature of that high-density chromatin layer to the experimentally observed steric hindrance of large molecules from the peripheral region of the nucleus. We relate our results and predictions to the available experimental data of nuclear chromatin distribution profiles, and lastly, discuss the implications and weaknesses of our model, together with future perspectives.

II. SCALING THEORY OF PERIPHERAL CHROMATIN

During interphase of eukaryotic cells, nuclear chromatin does not undergo microscopic changes. At this stage, individual chromosomes occupy distinct territories, but not all neighbor the nuclear boundary [2, 38]. This study only considers peripheral chromosomes, forming a straightforward polymer interface near the NE.

A. Assumptions and justifications

In polymer physics, a Kuhn segment of size $b = 2\ell_{\rm p}$ is defined as the largest segment of a polymer chain below which the polymer behaves as a rigid rod. The chemical composition of a polymer affects the persistence length $\ell_{\rm p}$, and thus, the Kuhn size b. However, polymer chains with distinctly different chemistry can exhibit universal conformational characteristics when considering chains composed of a sufficiently large number of Kuhn segments (*i.e.*, $N \gg 1$).

Considering the persistence length of chromatin on the order of $\ell_{\rm p} \sim 1$ kb to 10 kb [39–45], even the shortest reported LADs can correspond to $N_{\rm L} \sim 10^1$ to $\sim 10^2$ Kuhn segments respectively. These values are much shorter than a single chromosome (*i.e.*, with $N \sim 10^6$ Kuhn segments) but long enough to be statistically considered as a flexible polymer chain adsorbed on a surface.

Chromosomes are organized into chromatin fibers, which are protein-DNA complexes. One major protein complex organizing DNA into chromatin fiber is the histone octamer. Because the one-dimensional packing density of histone proteins varies along the fiber, chromatin is a highly heterogeneous polymer. Due to the variations in their histone packing densities [46, 47], heterochromatin and euchromatin can be structurally distinct and possibly have nonidentical persistence lengths [48]. For the same reason, values reported in the literature for chromatin persistence length vary largely, ranging between $\ell_{\rm p} \approx 30$ nm and $\ell_{\rm p} \approx 300$ nm [49–51]. Therefore, it is not straightforward to assign a clear difference between the persistence lengths of heterochromatin and euchromatin. Thus, we assume an identical Kuhn monomer size on the order of $b \simeq 10$ nm as a lower limit for heterochromatin-rich LADs and euchromatin-rich inter-LADs. Note that throughout the article, $\simeq$ signs denote scaling relations with neglected prefactors of order unity. Since scaling theories focus on the order magnitudes of the effects but not exact numbers, ignoring all prefactors on the order of unity, assuming equal Kuhn lengths for LADs and inter-LADs should not affect our scaling analysis. Hereon, by the term "*monomer*", we refer to a "*Kuhn monomer*" of size b.

We assume that the chromatin in its native nuclear environment can be modeled as a polymer solution in the concentrated regime. That is, the volume fraction of chromatin is $\phi > 0.1$. Single-particle tracking experiments reporting Rouse-type dynamics for the subsection of chromosomes support this assumption [52, 53].

We ignore the effects of electrostatic interactions since at physiological salt conditions (*i.e.*, $c_s \approx 100$ mM), chromatin could be treated as a neutral polymer for scaling purposes [49, 54]. In our calculations, there is also no selective attraction between chromatin segments that can lead to a phase separation.

Since the characteristic size of the chromosome is an order of magnitude smaller than the curvature radius of the nucleus (*i.e.*, $\sim 10^0$ μm *vs.* $\sim 10^1$ μm), we treat the inner NE surface as planar.

To distinguish between a surface-adsorbed and a non-adsorbed chromatin monomer, the adsorption of LAD segments to NE is modeled under the "*weak adsorption*" limit. The weak adsorption scheme also considers all weak interactions such as hydrogen bonding, ionic interactions, *etc.* Thus, instead of considering a subset of chromatin monomers anchored to NE by associated proteins with adsorption energies on the order of $-U \gg 1k_BT$, each chromatin monomer (whether LAD or inter-LAD) has an equal probability of interacting with the surface with an adsorption energy of $U \approx -\epsilon kT$, where $0 < \epsilon < 1$. LADs will be distinguished from inter-LADs *via* the formation of an adsorbed layer (see Sec. C

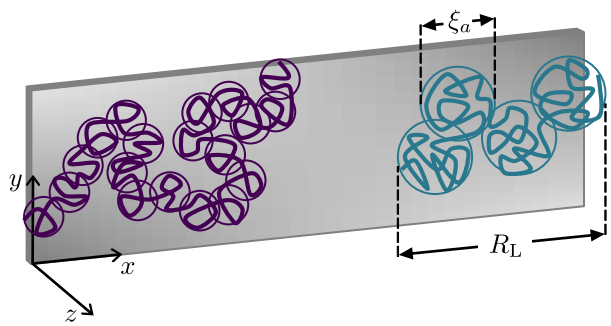

FIG. 2. Illustration of two isolated chains adsorbed on a flat surface. Both polymer chains have the same number $N_{\rm L}$ of Kuhn monomers of size b. The polymer on the left is adsorbed more strongly (with a larger ϵ) compared to the polymer on the right. For the more strongly adsorbed polymer on the left, number of monomers in an adsorption blob g_a and adsorption blob (mesh) size ξ_a are smaller [see Eqs. (1) and (3)], while number of blobs $N_{\rm L}/g_a$ and end-to-end size $R_{\rm L}$ are larger [see Eq. (4)].

below).

All parameters we consider are the averages of quantities that have Gaussian distributions. As argued above, an average number of Kuhn monomers per LAD and per inter-LAD ($N_{\rm L}$ and $N_{\rm I}$) are both considered to be much larger than unity. This regime of *long* polymers provides an excellent playground for scaling theories.

B. Single-chain adsorption model for an isolated LAD: adsorption blobs at the periphery

We begin our discussion by considering a single LAD composed of $N_{\rm L}$ monomers. While this discussion will provide insight for only an isolated LAD adsorbed on NE, it will help us introduce the concepts of chain adsorption, which will be used in the next section to describe the biologically relevant scenario of multiple independent LADs of a chromosome, overlappingly adsorbed on NE.

Consider an n-mer segment of a LAD, which is long enough to be considered as a flexible chain, but still much shorter than the whole LAD, *i.e.*, $1 \ll n \ll N_{\rm L}$. If the total attraction energy acting on all of its monomers is smaller than the thermal energy $k_{\rm B}T$, thermal fluctuations dominate the cumulative surface attraction. As a result, the n-mer segment has an unperturbed configuration; its root-mean-square size, $r(n) \simeq bn^{\nu}$, is the same as that of an unperturbed/non-adsorbed n-mer. The exponent ν depends on the solvent quality, polymer volume fraction, and the molecular architecture of the polymer. In the biologically relevant concentrated regime of our concern, $\nu = 1/2$ for linear polymers [55] and $\nu < 1/2$ for cyclic polymers [56–61].

As n increases, the number of contacts that the n-mer segment can form with the surface, and hence, the effect of surface attraction on the segment, increases. At a length scale

$$\xi_a \simeq b g_a^{\nu} \tag{1}$$

the cumulative adsorption energy of monomers in contact with the surface becomes on the order of thermal energy $k_{\rm B}T$. In Eq. 1, g_a is the number of monomers per adsorption blob. The monomer volume fraction within an adsorption blob can be written as $\phi_a \simeq b^3 g_a/\xi_a^3$. Using Eq. (1), we can write the volume fraction as a function of adsorption blob size as

$$\phi_a \simeq (\xi_a/b)^{(-3\nu+1)/\nu}\,. \tag{2}$$

Thus, the number of monomers in contact with the surface inside an adsorption blob is $(\phi_a/b^3) \times (\xi_a^2 b)$. Here, ϕ_a/b^3 is the number density of monomers inside an adsorption blob, and $\xi_a^2 b$ is the contact volume of the blob within a distance b to the surface. Thus, the adsorption energy of a blob is $(\epsilon k_{\rm B}T) \times (\phi_a/b^3) \times (\xi_a^2 b) \simeq \epsilon k_{\rm B}T\,(\xi_a/b)^{1/\nu-1}$. Equating this energy to thermal energy $k_{\rm B}T$, we obtain the size of an adsorption blob as

$$\xi_a \simeq b\epsilon^{-\nu/(1-\nu)}, \tag{3}$$

or the number of monomers in an adsorption blob as $g_a \simeq \epsilon^{-1/(1-\nu)}$.

There are $N_{\rm L}/g_a$ adsorption blobs along a single LAD. An isolated single LAD chain adsorbed on the nuclear periphery, therefore, behaves as a two-dimensional self-avoiding random walk of adsorption blobs on the surface (Fig. 2). Such a random walk of $N_{\rm L}/g_a$ steps, each of size ξ_a, has a root-mean-square end-to-end size of $R_{\rm L} \simeq \xi_a\,(N_{\rm L}/g_a)^{3/4}$ [62], from which, we obtain

$$R_{\rm L} \simeq b\epsilon^{(3/4-\nu)/(1-\nu)} N_{\rm L}^{3/4}, \tag{4}$$

via Eq. (3). As the surface attraction becomes stronger with increasing ϵ, the adsorption blob size ξ_a shrinks, see Eq. (3), but the number $N_{\rm L}/g_a$ of adsorption blobs per chain increases. The combined effect increases the two-dimensional end-to-end LAD size $R_{\rm L}$.

Assuming a median value of $N_{\rm L} \approx 10^3$ for a single LAD, we obtain $R_{\rm L} \simeq 100$ nm for the size of a single LAD after assuming $\epsilon = 1$. Assuming a weaker attraction (i.e., $\epsilon < 1$ decreases the LAD's size since the segment loses contact with the surface. Nevertheless, when the distance between neighboring adsorbed LADs is smaller than $R_{\rm L}$, those LADs interact by sterically repelling each other, and the above picture for isolated LADs loses validity. As will be discussed next, such a dense LAD environment alters polymer conformations and can lead to a steric environment for molecules diffusing through LADs.

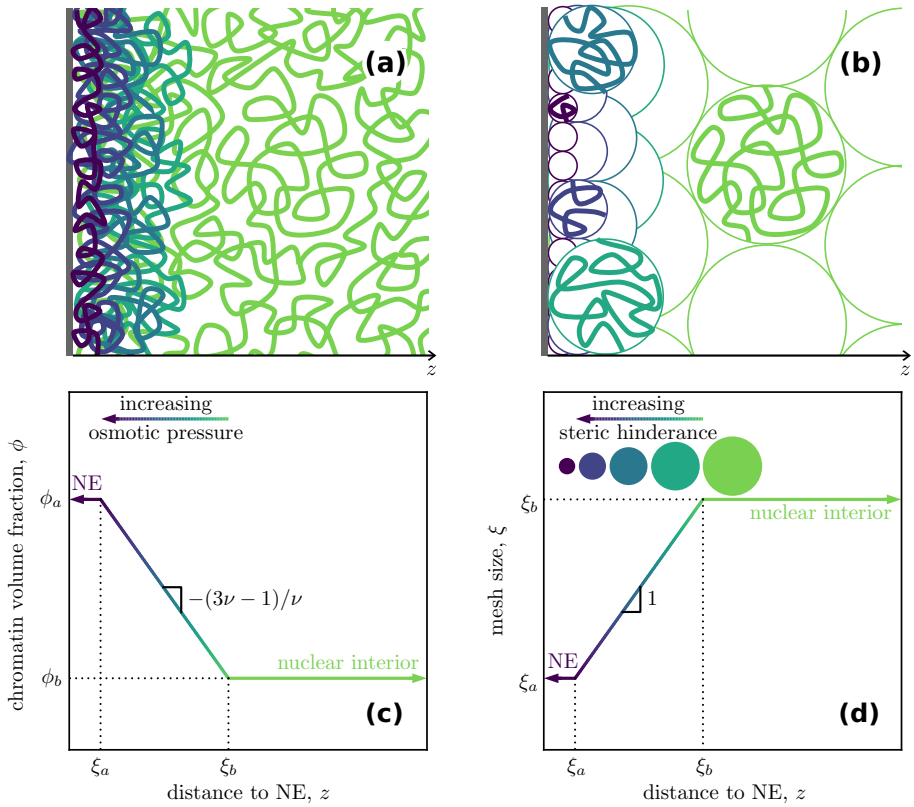

FIG. 3. a) and b) Illustration of multi-chain adsorption on a flat surface. Osmotic pressure on chain segments is color-coded from high pressure close to the surface (purple) to low pressure away from the surface (green). In (b), only several blobs are indicated by circles filled with chromatin segments or graphical simplicity. c) and d) The log-log plots of chromatin volume fraction ϕ and mesh (i.e., blob) size ξ as functions of distance z from the adsorbing surface. As the chromatin density decreases and the mesh size approaches its bulk value, the steric hindrance of proteins decreases, as depicted by spheres of varying sizes in (d).

C. Multi-chain adsorption model for a single chromosome

Consider an individual chromosome in contact with NE located at $z = 0$, where z defines the distance from the surface toward the nuclear interior. A certain fraction of the chromosome monomers should be in contact with the NE surface to form LADs, while the rest forms loops (e.g., inter-LADs depicted in Fig. 1). Experiments show that only $\sim 30\%$ of LADs identified by sequencing techniques are located at the nuclear periphery [7, 24, 63]. Thus, we can argue that there is insufficient space at the periphery to adsorb all LADs.

If LADs and inter-LADs are sufficiently long, we may treat them as independent chains. Accordingly, we suggest a molecular picture in which, near the nuclear periphery, many LADs compete for adsorption to the same limited surface space and sterically repel each other.

The adsorption energy is $\epsilon k_{\mathrm{B}}T$ per monomer at contact with NE. This surface attraction overcomes the steric repulsion between segments, and consequently, monomer concentration near the surface is at its maximum. Contrarily, monomers positioned away from the surface do have zero adsorption energy. As a result, the steric repulsion between segments becomes more dominant, favoring a less dense chromatin environment (Fig. 3a,c). Such a multi-chain adsorption scheme can be described by de Gennes' self-similar carpet model [64], in which the competition between steric chain-chain repulsion and chain-surface attraction determines the properties of the adsorbed polymer layer.

As discussed in the previous subsection, conformations of the adsorbed segments of this multi-chain structure are determined by the adsorption blobs of size ξ_a (i.e., Eq. (3)). The steric repulsion between chains defines a second length scale, the "*correlation blob*" size ξ, which is the average distance between chain segments of different chains. At the length scale of the correlation blob, the inter-chain steric repulsion energy is defined to be on the order of thermal energy $k_{\mathrm{B}}T$. Hence, at length scales below ξ, inter-chain steric repulsion is compensated by thermal energy, and chain segments have conformations unperturbed by the steric repulsion. That is to say, at length scales shorter than ξ, a chain segment and its subsections are unaware of other segments and behave as if it is isolated. Thus, the correlation blob size can be writ-

ten as $\xi \simeq bg^{\nu}$, where g is the number of monomers per blob.

The above definition of correlation blob size, ξ, gives the osmotic pressure (steric repulsion energy density) as $\pi \simeq k_{\mathrm{B}}T/\xi^3$. At the surface, since the steric interactions ($k_{\mathrm{B}}T$ per correlation blob) are compensated dominantly by the adsorption energy ($k_{\mathrm{B}}T$ per adsorption blob), the correlation blob coincides with the adsorption blob (*i.e.*, $\xi = \xi_a$). The high osmotic pressure, due to the high density of monomers close to the surface, is relaxed gradually as the distance z to the NE surface increases. Such a relaxation increases correlation length ξ and decreases volume fraction ϕ. Inside the "*bulk*" of the nucleus, far away from NE, the correlation blob size ξ_b and the volume fraction ϕ_b are both independent of the distance z, and they are related by [55]

$$\phi_b \simeq (\xi_b/b)^{(-3\nu+1)/\nu} \qquad \text{and} \qquad \xi_b \simeq b\phi_b^{\nu/(-3\nu+1)}. \quad (5)$$

The above relations also hold at an arbitrary distance z to the surface. The volume fraction of monomers inside a correlation blob is the same as the overall local volume fraction $\phi(z)$ at z, *i.e.*,

$$\phi \simeq b^3 g/\xi^3 \simeq (\xi/b)^{(-3\nu+1)/\nu}\,. \quad (6)$$

Hence, de Gennes' self-similar carpet can be seen as layers of correlation blobs of increasing size $\xi(z)$ with increasing distance z from the surface (Figs. 3b,d). The original model [64] argues a z-dependence for the correlation blob size, namely,

$$\xi(z) \simeq z \quad (7)$$

suggesting a linear relation between correlation length with the distance z until it reaches the bulk value at $z = \xi_b$. Plugging the above expression into Eq. (6) also provides a distance-dependent density profile:

$$\phi(z) \simeq (z/b)^{(-3\nu+1)/\nu}\,. \quad (8)$$

In summary, de Gennes's self-similar carpet model predicts the chromatin volume fraction and the correlation blob size profiles between nuclear boundary and bulk as follows

$$\phi(z) \simeq \begin{cases} \phi_a & , \quad z < \xi_a \\ \phi_a\,(z/\xi_a)^{(-3\nu+1)/\nu} & , \quad \xi_a < z < \xi_b\,, \\ \phi_b & , \quad \xi_b < z \end{cases} \quad (9)$$

$$\xi(z) \simeq \begin{cases} \xi_a & , \quad z < \xi_a \\ z & , \quad \xi_a < z < \xi_b\,, \\ \xi_b & , \quad \xi_b < z \end{cases} \quad (10)$$

Eqs. 9 and 10 are plotted in Figs. 3c and d in log-log scales. Notably, the correlation blob size ξ is proportional to mesh size (*i.e.*, the size sterically available to nuclear proteins). Thus, the smaller the ξ is, the stronger the steric hindrance near the nuclear boundary becomes. Figs. 3 highlights three distinct compartments of our model, each with a different chromatin density and mesh (correlation) size profiles. These three regions can interpreted as follows:

1. *In close proximity of the nuclear envelope*

At $z < \xi_a$, the surface is covered with a layer of adsorption blobs of size ξ_a. This high-density layer has a thickness of ξ_a given determined by the average size of adsorbed segments (Eq. (3) and can be interpreted as a *true* LAD layer. Since some LADs (or whole LADs) cannot find space on the surface to get adsorbed due to the finite space available, they would be pushed towards the nuclear interior by the high chromatin-osmotic pressure near the surface. Notably, such a layer can also provide extra strength to NE. [33]

2. *In between the nuclear periphery and the nuclear bulk*

As z increases along the interface region of $\xi_a < z < \xi_b$, the high pressure and density at the nuclear periphery relaxes, and the chromatin density approaches its bulk values 3c. The relaxation of surface effects increases correlation length ξ with increasing z. This increasing correlation size can allow large molecules to diffuse through the dense chromatin structure. In principle, layers of blobs in this interface region contain subsections of both LADs and inter-LADs.

3. *Inside the nuclear bulk*

Far away from the nuclear periphery at $z > \xi_b$, the abovementioned pressure relaxation is complete. The chromatin sections in this region do not *feel* the adsorbing surface from this distance. Here, the only effect of NE on the chromatin is the nuclear confinement. Experiments identified this interior region with low chromatin density and high transcriptional activity [4, 6, 25, 29]. This region is manifested by a surface-independent mesh size (correlation length) ξ_b, which is larger than the mesh size near the surface.

III. COMPARISON TO EXPERIMENTAL DATA FROM LITERATURE

To obtain a quantitative validation of our model, we facilitate the experimentally available data published in the literature. First, we compare our scaling predictions with the chromatin density profiles for eukaryotic cell types (Fig. 4 and Table I).

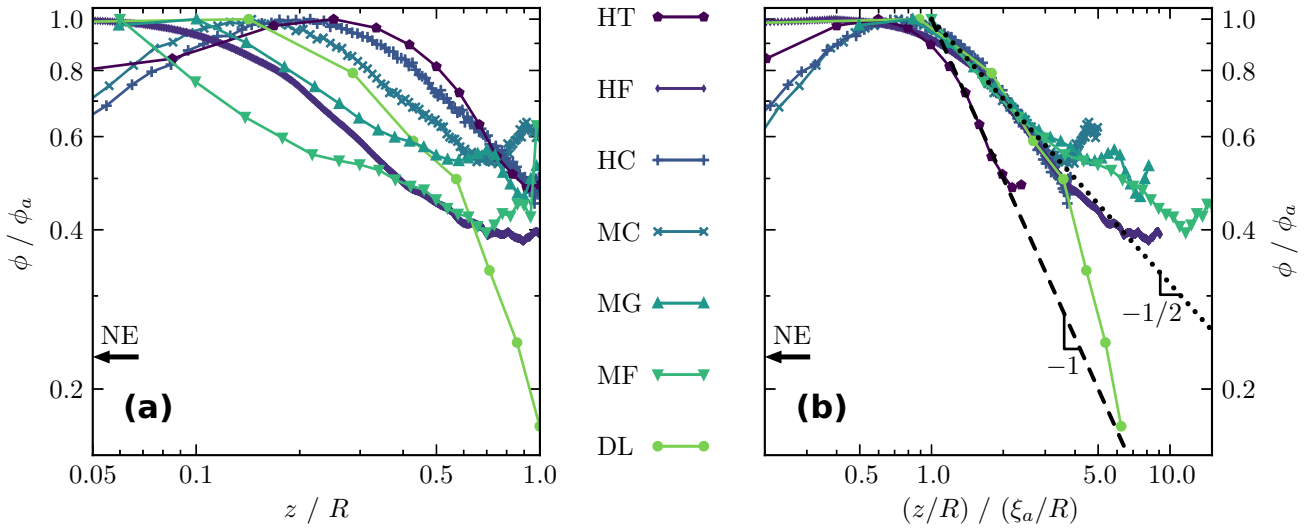

FIG. 4. Log-log plots for the dependence of chromatin volume fraction ϕ on distance to nuclear periphery z. Data are from various eukaryotic cell types; Table I for abbreviations. In both panels, ϕ data is scaled by the maximum measured volume fraction ϕ_a for that cell type. In the left panel, z is scaled by cell radius R, such that $z/R = 1$ is at the nuclear center. The decrease in chromatin density close to the nuclear periphery at small z/R, is due to a depletion region not considered in the theory. In the right panel, z/R is scaled with ξ_a/R to obtain a data collapse in accordance with Eq. (11). Fitting parameteres for ξ_a/R are given in Table I. The dashed and dotted lines show our predictions of $\phi/\phi_a \simeq (z/\xi_a)^{-1}$ and $\phi/\phi_a \simeq (z/\xi_a)^{-1/2}$; see Fig. 3c and Eq. (11) with $\nu = 1/2$ and $\nu = 2/5$ respectively. The data points are joined to guide the eye.

In literature, the nuclear chromatin density profiles were often reported in the units of fluorescence intensity or arbitrary units as a function of nuclear radial distance. Therefore, to compare our results summarized in Eq. 9 with such data, we normalize the density axis by the maximum value of the signal for the corresponding cell type. The maximum value is matched to the density value near the surface in our model (i.e., ϕ_a). Then, we compare the rescaled data with our normalized density distribution (i.e., ϕ/ϕ_a) (Fig. 4a).

In general, as shown in Fig. 4a, decreasing chromatin concentration with increasing distance from the nuclear periphery is a common hallmark of the density profiles in all simulations and experiments [35, 65–73] and agrees well with our model, see Eq. (9) and Fig. 3c. This can be seen more quantitatively in the master curve combining all the available data by using the expression

$$\frac{\phi(z)}{\phi_a} \simeq \left(\frac{z/R}{\xi_a/R}\right)^{(-3\nu+1)/\nu} \tag{11}$$

for $\xi_a < z < \xi_b$. To obtain the overlap in Fig. 4b, we use ξ_a/R as a free fit parameter in Eq. 9 for all cell types (see Table I for the fit values). We observe that the thickness of the LAD layer relative to the nuclear radius is in the range of about $\xi_a/R \simeq 0.1 - 0.2$, which agrees well with high-resolution microscopy images [24, 31, 63]. The only exception is the human T-cell, for which we predict a ξ_a/R value of about 40% (Table I). Also, note that data for this cell type is singled out from the other collapsed data sets in Fig. 4b.

Code	Ref.	Cell type	ξ_a/R
HT	[65]	Human T-cell	0.42
HF	[66]	Human fibroblast	0.11
HC	[67]	Human cardiomyocyte	0.26
MC	[67]	Mouse cardiomyocyte	0.20
MG	[68]	Mouse ganglion†	0.12
MF	[68]	Mouse fibroblast†	0.06
DL	[69]	Drosophila larval muscle	0.16

TABLE I. Fit parameters, ξ_a/R, used to collapse the experimental data on a master curve in Fig. 4b. († Includes only gene-poor heterochromatin, but not the gene-rich euchromatin.)

The data in Fig. 4b highlights a concentration decay from the nuclear surface to the bulk. However, for the human T-cell, this decay is stronger; while our model predicts $\phi/\phi_a = (z/\xi_a)^{-1}$ for the human T-cell for linear chains of $\nu = 1/2$, all other data can be collapsed onto a universal line of $\phi/\phi_a = (z/\xi_a)^{-1/2}$ away from the nuclear center. This expression is obtained if an exponent of $\nu = 2/5$ is chosen for the statistical conformation of the LAD and inter-LAD segments; see Eq. (9). While the exponent $\nu = 2/5$ describes the data relatively well, it is larger than some predictions (i.e., $\nu = 1/3$) [56, 61], but consistent with others [57–60]. Alternatively, the average of size LADs data could reflect a transition regime from a $\nu = 2/5$-controlled regime to a regime of more compact polymer sizes (i.e., $\nu = 1/3$) [74, 75].

Next, we compare the correlation lengths that we pre-

dict with the available experimental data reporting the effective porosity of nuclear chromatin. By microinjecting fluorescent-labeled dextran probe molecules of varying molecular mass M into interphase HeLa nuclei, Görisch *et al.* correlated the nuclear distribution of such particles with the nuclear porosity near and away from the periphery [35]. While small dextran molecules (i.e., $d \lessapprox 20$ nm) with $M \leq 77$ kDa can diffuse close to the nuclear periphery, larger molecules cannot. For those larger molecules, the dextran density increases away from the NE and levels off inside the nuclear bulk. This finding is in qualitative agreement with our predictions of decreasing mesh size near the surface given by

This finding is in qualitative agreement with our predictions for the mesh size [see Eq. (6)],

$$\xi(z) \simeq \begin{cases} b\,[\phi(z)]^{-2} & , \ \nu = 2/5 \\ b\,[\phi(z)]^{-1} & , \ \nu = 1/2 \end{cases}. \tag{12}$$

Note that the above predictions are much stronger than the inverse square root dependence obtained by considering chromatin as hexagonal packed crystals [76].

The smallest length scale in our model is the Kuhn length (or the persistence diameter), $b = 2\ell_p$. Such a scaling model can only make limited predictions about the phenomena related to length scales smaller than b. One such prediction is that since the Kuhn length defines the size of the smallest loops that can be formed by the polymer chain inside the dense chromatin environment, any molecule smaller than b can find pores to diffuse along. This simple picture is adequate to describe the smallest mesh size of $b \approx 20$ nm observed by Görisch *et al.* close to the nuclear periphery. In fact, this is on the order of the Kuhn size of chromatin, which $b \simeq 10$ nm.

A second steric barrier in the experiments observed is the mesh size of $\xi \approx 60$ nm, which can be inferred as the size ξ_a of the adsorption blobs of our model [35, 76]. For the HeLa nuclei of radius $R \approx 1$ μm, this adsorption blob size value leads to $\xi_a/R \approx 0.06$, in accord with the range of values presented in Table I. We note that by plugging the values $\xi_a \approx 60$ nm and $b \approx 20$ nm into Eq. (1), we obtain the number of Kuhn monomers in an adsorption blob as $g_a \simeq 10$ for both linear ($\nu = 1/2$) and cyclic ($\nu = 2/5$) chains. Recalling that our scaling theory assumes $g_a \gg 1$, a value of $g_a \simeq 10$ is at the limiting boundary of the validity of our model.

Finally, from this relative thickness ξ_a/R, we predict the relative nuclear volume of the LAD layer as

$$V_{\rm LAD}/V \simeq \xi_a/R, \tag{13}$$

where $V \simeq R^3$ is the nuclear volume. For a nuclear radius of around $R \approx 5$ μm, using the values in Table I, we obtain a relative volume of the LAD layer in the range $V/V_{\rm LAD} \simeq 10{-}20\%$, with an average LAD layer thickness of $\xi_a < 1$ μm. This prediction agrees well with high-resolution microscopy images [24, 31, 63].

IV. DISSCUSSION

By revisiting de Gennes' self-similar carpet model, we argue that lamina-associated chromatin domains can be considered as multiple independent chain segments (of a chromosome) attracted to a surface with an energy of $U = -\epsilon k_{\rm B}T$ per adsorbed Kuhn monomer. In our calculations, we assume chromatin layers adjacent to the surface with a thickness ξ_a are all occupied by LADs.

In reality, for short LAD and long inter-LAD segments, only a fraction of the surface is covered by isolated LADs that form adsorption blobs of size ξ_a. In contrast, the rest of the nuclear surface is covered by inter-LADs of correlation length ξ_b. However, DamID and ChIP-seq experiments associate $\sim 40\%$ of the genome as LADs [7, 9, 77]. For such long LADs, the layers close to the nuclear periphery must be filled almost entirely with adsorption blobs corresponding to LAD chains, per our assumptions.

Our calculations do not distinguish between chromatin sections permanently tethered to NE and those interacting weakly with the periphery. Nevertheless, the statistical nature of the scaling analyses favors surface localization limited by steric repulsion between LAD segments. Thus, the detailed nature of the surface localization does not change the outcome and provides relatively good chromatin distributions as compared to experiments. However, distinguishing tethering from weak attraction or varying the chain stiffness affected the contact probabilities at ~ 100 kb scale [45], but averaging over many segments in contact with NE can provide a picture similar to our predictions. It is also intuitive to think that more permanent contacts with NE can give LADs structural properties such as those observed in cyclic polymer brushes [78–80] or a combination of a brush and de Gennes' carpet [81]. In fact, assuming a cyclic architecture for the inter-LADs that are attached from both ends to NE and protrude towards the nuclear interior, forming loops, explains the chromatin density profile data for various eukaryotic cells (Fig. 4).

In fact, an inter-LAD in between two consecutive LADS, can be attached to NE from both ends and effectively could have a cyclic polymer topology. In addition, on smaller length scales, chromatin loops are formed by the interactions between topologically associated domains along the chromosome [5, 6, 10, 25, 82, 83]. Hence, the peripheral chromatin could be modeled as a cyclic polymer that can be described by the exponent $\nu = 2/5$. In that sense, the outlier data point in Fig. 4b, human T-cells, can be rationalized by the argument that the inter-LADs in human T-cells are tethered to NE at distant positions, and as such, the peripheral chromatin in between these tethering points cannot be treated as a concentrated solution of cyclic chains but as linear chains. Moreover, the T-cell chromatin distribution decreasing strongly with surface separation (Fig. 4b) may also be due to the constrained release of lamina-associated enhancers and genes from the nuclear envelope, as observed during Jurkat T-cell activation [84], which changes the 3d

organization of the genome.

Our model explains the steric hindrance of large molecules from the nuclear periphery. Adsorption of LADs to NE generates a structurally distinct layer of chromatin with a mesh size smaller than in the bulk of the nucleus (*i.e.*, $\xi < \xi_b$). This picture leads to an effective hindrance mechanism. The smallest mesh size is ξ_a at the proximity of NE. The same ξ_a defines the thickness of the densest layer on the surface, *i.e.*, the thickness of the LAD layer. As the distance to NE increases, the mesh size grows towards that inside the nuclear bulk (ξ_b). This hindrance can exclude large proteins of transcription machinery from the LADs and reinforce the suppressive environment of LADs via this non-specific effect that does not depend on the nucleic acid sequence. The exact mechanism can allow larger mesh sizes, for instance, near the nuclear pore complexes around which euchromatin is relatively sparse, allowing more transcriptional activity near LADs. The hindrance of very small molecules (smaller than the persistence diameter of chromatin, ~ 20 nm) cannot be explained by the mechanism of growing mesh size ξ, but could be due to the convergence of nucleosome into an effective (dense) melt (e.g., polymer brush [81]). Consistently, a recent study [85] discusses that surface-attached LADs have less gene activity than non-attached LADs, which reside at the interface between the so-called "compartment A" and "compartment B". This result supports the increasing mesh size along the interface region. Proteins regulating the genetic machinery cannot reach the dense layer of surface-attached LADs, while they reach the non-attached LAD segments of the larger mesh size.

The polymer model does not separate LADs and inter-LADs. Yet, one can conclude that chromatin sections away from the nuclear periphery are of inter-LAD nature implicitly. A more detailed model can separate these two chromatin types, possibly considering copolymers with two different persistence lengths [48]. Nevertheless, we anticipate that within the limits of valid biological parameters, decreasing steric hindrance and decreasing chromatin density towards the nuclear interior will be preserved even in a more complex model. This is also evident from the experimental data in which more compact chromocenter regions of the genome have a mild effect on chromatin distribution, albeit these faces cause higher heterochromatin concentration near their surface. (See, *e.g.*, MG and MF data in Fig. 4b and the corresponding Ref. [68].)

Overall, our theoretical approach demonstrates that organizing a meters-long genome inside a micron-size nucleus can require the facilitation of various polymer structures, many of which have been studied extensively in the context of synthetic polymers. Revealing the structural complexity of genome organization can help us extend our knowledge of the relationship between 3d chromosome organization, genetic regulation, and nuclear morphology.

ACKNOWLEDGMENTS

We thank J. Paturej for the valuable discussions. This work has been supported by the National Science Center, Poland (Grant Polonez Bis No. 2021/43/P/ST3/01833) and The Council of Science and Technology of Turkey (TUBITAK) Grant no 122F309.

[1] T. Cremer and C. Cremer, Nature Reviews Genetics **2**, 292 (2001).
[2] C. Weierich, A. Brero, S. Stein, J. von Hase, C. Cremer, T. Cremer, and I. Solovei, Chromosome Research **11**, 485 (2003).
[3] M. R. Branco and A. Pombo, TRENDS in Cell Biology **17**, 127 (2007).
[4] A. Buchwalter, J. M. Kaneshiro, and M. W. Hetzer, Nature Reviews Genetics **20**, 39 (2019).
[5] L. A. Mirny, M. Imakaev, and N. Abdennur, Current Opinion in Cell Biology **58**, 142 (2019).
[6] H. Zheng and W. Xie, Nature Reviews Molecular Cell Biology **20**, 535 (2019).
[7] N. Briand and P. Collas, Genome Biology **21**, 85 (2020).
[8] D. E. Olins and A. L. Olins, Nature Reviews Molecular Cell Biology **4**, 809 (2003).
[9] D. Peric-Hupkes, W. Meuleman, L. Pagie, S. W. M. Bruggeman, I. Solovei, W. Brugman, S. Gräf, P. Flicek, R. M. Kerkhoven, M. van Lohuizen, M. Reinders, L. Wessels, and B. van Steensel, Molecular Cell **38**, 603 (2010).
[10] A. Pombo and N. Dillon, Nature Reviews Molecular Cell Biology **16**, 245 (2015).
[11] E. Wegel and P. Shaw, Chromosoma **114**, 331 (2005).
[12] F. Erdel, Current Opinion in Genetics and Development **61**, 62 (2020).
[13] B. Burke and C. L. Stewart, Nature Reviews Molecular Cell Biology **3**, 575 (2002).
[14] C. J. Hutchison, Nature Reviews Molecular Cell Biology **3**, 848 (2002).
[15] K. Hoffmann, C. K. Dreger, A. L. Olins, D. E. Olins, L. D. Shultz, B. Lucke, H. Karl, R. Kaps, D. Müller, A. Vayá, J. Aznar, R. E. Ware, N. S. Cruz, T. H. Lindner, H. Herrmann, A. Reis, and K. Sperling, Nature Genetics **31**, 410 (2002).
[16] L. D. Shultz, B. L. Lyons, L. M. Burzenski, B. Gott, R. Samuels, P. A. Schweitzer, C. Dreger, H. Herrmann, V. Kalscheuer, A. L. Olins, D. E. Olins, K. Sperling, and K. Hoffmann, Human Molecular Genetics **12**, 61 (2003).
[17] P. Taimen, K. Pfleghaar, T. Shimi, D. Möller, K. Ben-Harush, M. R. Erdos, S. A. Adam, H. Herrmann, O. Medalia, F. S. Collins, A. E. Goldman, and R. D. Goldman, Proceedings of the National Academy of Sciences **106**, 20788 (2009).
[18] K. B. Pfleghaar, P. Taimen, V. Butin-Israeli, T. Shimi, S. Langer-Freitag, Y. Markaki, A. E. Goldman, M. Wehnert, and R. D. Goldman, Nucleus **6**, 66 (2015).

[19] D. Zink, A. H. Fischer, and J. A. Nickerson, Nature Reviews Cancer **4**, 677 (2004).

[20] D. M. Carone and J. B. Lawrence, Seminars in Cancer Biology **23**, 99 (2013).

[21] E. Lieberman-Aiden, N. L. van Berkum, L. Williams, M. Imakaev, T. Ragoczy, A. Telling, I. Amit, P. J. S. Bryan R. Lajoie, M. O. Dorschner, R. Sandstrom, B. Bernstein, M. A. Bender, M. Groudine, A. Gnirke, J. Stamatoyannopoulos, L. A. Mirny, E. S. Lander, and J. Dekker, Science **326**, 289 (2009).

[22] E. Lund, A. R. Oldenburg, and P. Collas, Nucleic Acids Research **42**, e92 (2014).

[23] B. van Steensel, J. Delrow, and S. Henikoff, Nature Genetics **27**, 304 (2001).

[24] J. Kind, L. Pagie, H. Ortabozkoyun, S. Boyle, S. S. de Vries, H. Janssen, M. Amendola, L. D. Nolen, W. A. Bickmore, and B. van Steensel, Cell **153**, 178 (2013).

[25] I. Jerković and G. Cavalli, Nature Reviews Molecular Cell Biology **22**, 511 (2021).

[26] L. Guelen, L. Pagie, E. Brasset, W. Meuleman, M. B. Faza, W. Talhout, B. H. Eussen, A. de Klein, L. Wessels, W. de Laat, and B. van Steensel, Nature **453**, 948 (2008).

[27] W. Meuleman, D. Peric-Hupkes, J.-B. B. Jop Kind, L. Pagie, M. Kellis, M. Reinders, L. Wessels, and B. van Steensel, Genome Research **23**, 270 (2013).

[28] T. Rønningen, A. Shah, A. R. Oldenburg, K. Vekterud, E. Delbarre, J. Ø. Moskaug, and P. Collas, Genome Research **25**, 1825 (2015).

[29] L. Chang, M. Li, S. Shao, C. Li, S. Ai, B. Xue, Y. Hou, Y. Zhang, R. Li, X. Fan, A. He, C. Li, and Y. Sun, Protein and Cell **13**, 258 (2020).

[30] X. Wong, J. A. Cutler, V. E. Hoskins, M. Gordon, A. K. Madugundu, A. Pandey, and K. L. Reddy, Life Science Alliance **4**, e202000774 (2021).

[31] B. van Steensel and A. S. Belmont, Cell **169**, 780 (2017).

[32] J. C. Harr, T. R. Luperchio, X. Wong, E. Cohen, S. J. Wheelan, and K. L. Reddy, Journal of Cell Biology **208**, 33 (2015).

[33] A. Janssen, S. U. Colmenares, and G. H. Karpen, Annual Review of Cell and Developmental Biology **34**, 265 (2018).

[34] J. Madsen-Østerbye, A. Bellanger, N. M. Galigniana, and P. Collas, Frontiers in Cell and Developmental Biology **10**, 913458 (2022).

[35] S. M. Görisch, M. Wachsmuth, K. F. Tóth, P. Lichter, and K. Rippe, Journal of Cell Science **118**, 5825 (2005).

[36] Y. Levy, J. N. Onuchic, and P. G. Wolynes, Journal of the American Chemical Society **129**, 738 (2007).

[37] A. Erbaş, D. Horinek, and R. R. Netz, Journal of the American Chemical Society **134**, 623 (2012).

[38] T. Cremer and M. Cremer, Cold Spring Harbor Perspectives in Biology **2**, a003889 (2010).

[39] Y. Cui and C. Bustamante, Proceedings of the National Academy of Sciences **97**, 127 (2000).

[40] J. Dekker, K. Rippe, M. Dekker, and N. Kleckner, Science **295**, 1306 (2002).

[41] S. Jun, J. Herrick, A. Bensimon, and J. Bechhoefer, Cell Cycle **3**, 223 (2004).

[42] K. Bystricky, P. Heun, L. Gehlen, J. Langowski, and S. M. Gasser, Proceedings of the National Academy of Sciences **101**, 16495 (2004).

[43] K. S. Bloom, Chromosoma **117**, 103 (2008).

[44] P. R. Cook and D. Marenduzzo, Journal of Cell Biology **186**, 825 (2009).

[45] A. Brunet, N. Destainville, and P. Collas, Nucleus **12**, 6 (2021).

[46] G. J. Thorn, C. T. Clarkson, A. Rademacher, H. Mamayusupova, G. Schotta, K. Rippe, and V. B. Teif, Nature Communications **13**, 1861 (2022).

[47] M. A. Ricci, C. Manzo, M. F. García-Parajo, M. Lakadamyali, and M. P. Cosma, Cell **160**, 1145 (2015).

[48] M. Girard, M. O. de la Cruz, J. F. Marko, and A. Erbaş, bioRχiv **12.01.403832**, 1 (2020).

[49] J. Langowski, The European Physical Journal E **19**, 241 (2006).

[50] H. Hajjoul, J. Mathon, H. Ranchon, I. Goiffon, J. Mozziconacci, B. Albert, P. Carrivain, J.-M. Victor, O. Gadal, K. Bystricky, and A. Bancaud, Genome Research **23**, 1829 (2013).

[51] D. Kolbin, B. L. Walker, C. Hult, J. D. Stanton, D. Adalsteinsson, M. G. Forest, and K. Bloom, Genes **14**, 2193 (2023).

[52] S. S. Ashwin, T. Nozaki, K. Maeshima, and M. Sasai, Proceedings of the National Academy of Sciences **116**, 19939 (2019).

[53] R. Benelli and M. Weiss, Biophysical Journal **121**, 2684 (2022).

[54] J. F. Marko, Journal of Molecular Biology **432**, 621 (2020).

[55] M. Rubinstein and R. H. Colby, *Polymer Physics* (Oxford University Press, Oxford, Great Britain, 2003).

[56] M. E. Cates and J. M. Deutsch, Journal de Physique France **47**, 2121 (1986).

[57] S. Brown and G. Szamel, The Journal of Chemical Physics **109**, 6184 (1998).

[58] M. Müller, J. P. Wittmer, and J.-L. Barrat, Europhysics Letters **52**, 406 (2000).

[59] K. Hur, C. Jeong, R. G. Winkler, N. Lacevic, R. H. Gee, and D. Y. Yoon, Macromolecules **44**, 2311 (2011).

[60] C. Jeong and J. F. Douglas, Macromolecular Theory and Simulations **26**, 1700045 (2017).

[61] A. Rosa and R. Everaers, Phys. Rev. Lett. **112**, 118302 (2014).

[62] B. Nienhuis, Physical Review Letters **49**, 1062 (1982).

[63] J. Paulsen, M. Sekelja, A. R. Oldenburg, A. Barateau, N. Briand, E. Delbarre, A. Shah, A. L. Sørensen, C. Vigouroux, B. Buendia, and P. Collas, Genome Biology **18**, 21 (2017).

[64] P. G. de Gennes, Macromolecules **14**, 1637 (1981).

[65] D. Amiad-Pavlov, D. Lorber, G. Bajpai, A. Reuveny, F. Roncato, R. Alon, S. Safran, and T. Volk, Science Advances **7**, eabf6251 (2021).

[66] Y. Li, V. Agrawal, R. K. A. Virk, E. Roth, W. S. Li, A. Eshein, J. Frederick, K. Huang, L. Almassalha, R. Bleher, M. A. Carignano, I. Szleifer, V. P. Dravid, and V. Backman, Scientific Reports **12**, 12198 (2022).

[67] B. Seelbinder, S. Ghosh, S. E. Schneider, A. K. Scott, A. G. Berman, C. J. Goergen, K. B. Margulies, K. C. B. Jr., E. Casas, A. R. Swearingen, J. Brumbaugh, S. Calve, and C. P. Neu, Nature Biomedical Engineering **5**, 1500 (2021).

[68] I. Solovei, M. Kreysing, C. Lanctôt, S. Kösem, L. Peichl, T. Cremer, J. Guck, and B. Joffe, Cell **137**, 356 (2009).

[69] D. Amiad-Pavlov, C. P. Unnikannan, D. Lorber, G. Bajpai, T. Olender, E. Stoops, A. Reuveny, S. Safran, and T. Volk, Cells **12**, 932 (2023).

[70] A. Poleshko, C. L. Smith, S. C. Nguyen, P. Sivaramakrishnan, K. G. Wong, J. I. Murray, M. Lakadamyali, E. F. Joyce, R. Jain, and J. A. Epstein, eLife **8**, e49278 (2019).

[71] A. Maji, J. A. Ahmed, S. Roy, B. Chakrabarti, and M. K. Mitra, Biophysical Journal **118**, 3041 (2020).

[72] G. Bajpai, D. A. Pavlov, D. Lorber, T. Volk, and S. Safran, eLife **10**, e63976 (2021).

[73] S. Brahmachari, V. G. Contessoto, M. D. Pierro, and J. N. Onuchic, Nucleic Acids Research **50**, 4258 (2022).

[74] M. Lang, J. Fischer, and J.-U. Sommer, Macromolecules **45**, 7642 (2012).

[75] T. Ge, S. Panyukov, and M. Rubinstein, Macromolecules **49**, 708 (2016).

[76] T. Weidemann, M. Wachsmuth, T. A. Knoch, G. Müller, W. Waldeck, and J. Langowski, Journal of Molecular Biology **334**, 229 (2003).

[77] A. Poleshko, P. P. Shah, M. Gupta, A. Babu, M. P. Morley, L. J. Manderfield, J. L. Ifkovits, D. Calderon, H. Aghajanian, J. E. Sierra-Pagán, Z. Sun, Q. Wang, L. Li, N. C. Dubois, E. E. Morrisey, M. A. Lazar, C. L. Smith, J. A. Epstein, and R. Jain, Cell **171**, 573 (2017).

[78] A. Erbaş and J. Paturej, Soft Matter **11**, 3139 (2015).

[79] J. Paturej and A. Erbaş, Physical Biology **20**, 056004 (2023).

[80] S. Milner, T. Witten, and M. Cates, Macromolecules **21**, 2610 (1988).

[81] T. Ge and M. Rubinstein, Macromolecules **48**, 3788 (2015).

[82] S. S. P. Rao, M. H. Huntley, N. C. Durand, E. K. Stamenova, I. D. Bochkov, J. T. Robinson, A. L. Sanborn, I. Machol, A. D. Omer, E. S. Lander, and E. L. Aiden, Cell **159**, 1665 (2014).

[83] M. J. Rowley and V. G. Corces, Nature Reviews Genetics **19**, 789 (2018).

[84] M. I. Robson, J. I. de las Heras, R. Czapiewski, A. Sivakumar, A. R. W. Kerr, and E. C. Schirmer, Genome Research **27**, 1126 (2017).

[85] P. P. Shah, K. C. Keough, K. Gjoni, G. T. Santini, R. J. Abdill, N. M. Wickramasinghe, C. E. Dundes, A. Karnay, A. Chen, R. E. A. Salomon, P. J. Walsh, S. C. Nguyen, S. Whalen, E. F. Joyce, K. M. Loh, N. Dubois, K. S. Pollard, and R. Jain, Genome Biology **24**, 16 (2023).